Research Square

Preprints are preliminary reports that have not undergone peer review.
They should not be considered conclusive, used to inform clinical practice,
or referenced by the media as validated information.

A Baseline-Normalized Suspension Degradation Index for Shock Absorber Health Monitoring

Geetha Mani

geetha.mani@vit.ac.in

Vellore Institute of Technology

Article

Keywords: suspension degradation index, shock absorber fault diagnosis, suspension health monitoring, single-sensor monitoring, median absolute deviation, quarter-car model

Posted Date: November 12th, 2026

DOI: https://doi.org/10.21203/rs.3.rs-11482941/v1

License: This work is licensed under a Creative Commons Attribution 4.0 International License.
Read Full License

Additional Declarations: No competing interests reported.

A Baseline-Normalized Suspension Degradation Index for Shock Absorber Health Monitoring

Geetha Mani

School of Electrical Engineering, Vellore Institute of Technology, Vellore Campus, India, Vellore 632014

Corresponding author: Geetha Mani, geethamr@gmail.com; geetha.mani@vit.ac.in

Abstract

Shock absorber degradation develops gradually and is difficult to identify before significant damping loss occurs. Most existing diagnostic methods depend on multiple sensors, accurate system models, or supervised learning trained on labelled fault data. A baseline-normalized Suspension Degradation Index (SDI) is proposed for single-sensor suspension health monitoring. The SDI tracks resonance-band chassis vibration and quantifies damper degradation relative to a healthy baseline established using the median and median absolute deviation. False alarms caused by transient road disturbances are suppressed through a persistence criterion, while a wear-dependent thermal model provides an independent indication of progressive damper degradation. The two indicators are combined into one health index. The method is evaluated using a quarter-car model excited by an ISO 8608 Class-C road profile containing a transient pothole and progressive damping degradation from 1500 to 450 N·s/m. The persistence criterion rejects the pothole response without producing a false alarm, whereas the thermal indicator detects progressive wear. Across 25 independent road realizations, the combined framework achieved a 100% overall detection rate, and the thermal indicator became active only when damping degradation exceeded approximately 40%. The approach requires only one chassis-mounted accelerometer and simple statistical processing, which suits practical monitoring and future experimental implementation.

Keywords: suspension degradation index; shock absorber fault diagnosis; suspension health monitoring; single-sensor monitoring; median absolute deviation; quarter-car model

1. Introduction

Vehicle suspension systems play a vital role in maintaining ride comfort, handling stability, and tire–road contact under varying road conditions. Hydraulic shock absorbers dissipate vibration energy and control the oscillatory motion induced by road irregularities. Over prolonged operation, shock absorbers gradually deteriorate because of hydraulic fluid leakage, seal wear, valve fatigue, gas-pressure loss, and mechanical ageing. This deterioration reduces damping capability, leading to increased body vibration, degraded handling performance, and accelerated tire wear. Since these changes occur progressively, early-stage

faults often remain undetected during normal driving. Consequently, reliable condition-monitoring techniques are essential for early fault detection and improved vehicle safety.

Existing suspension fault-diagnosis methods can broadly be classified into model-based, signal-processing, machine-learning, and condition-monitoring approaches. Model-based methods generate residuals by comparing measured responses with a mathematical representation of the suspension system. For example, an unknown-input observer combined with a support vector machine has been used to detect suspension sensor faults under unknown road-surface conditions [1]. Reduced-order fault-detection filters and Takagi–Sugeno fuzzy observers have also been developed for active suspension systems to improve robustness while reducing computational requirements [2], [3]. Although these approaches provide physically interpretable fault indicators, their performance depends on the accuracy of the adopted model and its ability to represent variations in operating conditions.

Other approaches exploit suspension transmissibility and dynamic-response characteristics to identify damper degradation. Sammier *et al.* proposed a fault-detection method for an automotive magnetorheological damper based on suspension transmissibility and road-frequency estimation [4]. Słomczyński *et al.* investigated damaged suspension components using a quarter-car model with a magnetorheological damper and backstepping control [5]. Such model- and response-based approaches can provide useful information about suspension condition; however, their implementation may require additional system information, model parameters, or controlled excitation conditions.

Signal-processing methods provide an alternative by extracting fault-sensitive characteristics directly from measured vibration responses. Wavelet-based analysis has been applied to passive suspension fault detection [6], while wavelet-packet features have been investigated for identifying degradation in railway suspension components [7]. More recently, domain-adaptation techniques have been used to improve suspension fault diagnosis under varying operating speeds [8]. These approaches can capture transient and frequency-dependent changes in suspension behaviour, but time–frequency decomposition and associated feature extraction may impose greater computational requirements than fixed-filter statistical processing.

Machine-learning methods have also been increasingly investigated for suspension fault diagnosis. Transfer learning has been combined with vibration representations for suspension fault detection [9], while decision-tree classifiers have been applied to vibration features from automobile suspension systems [10]. A weightless neural network has also been investigated for suspension fault diagnosis with emphasis on rapid classification [11]. These methods can provide effective classification of multiple fault conditions, but their application generally requires representative fault data covering the operating and degradation conditions of interest. The availability of labelled data and the computational requirements of trained models can therefore become important considerations for practical embedded implementation.

Temperature-based monitoring provides another route for assessing shock absorber condition. A patented monitoring device determines shock-absorber condition and wear from temperature measurements [12], while calorimetry-based monitoring has been investigated for estimating the age of

vehicle shock absorbers [13]. Experimental studies have further examined temperature rise in adjustable damping shock absorbers [14] and the influence of temperature on hydraulic shock-absorber damping characteristics [15]. More recent work has considered the combined influence of temperature and technical condition on hydraulic shock absorbers [16]. These studies demonstrate the usefulness of thermal information for suspension health monitoring, but the behaviour of a simple wear-dependent thermal indicator under random road excitation and transient disturbances requires further investigation.

These limitations highlight the gap between diagnostic methods demonstrated under specific laboratory or controlled modelling conditions and approaches suitable for practical deployment on low-cost embedded platforms. A single-sensor approach capable of assessing suspension condition without requiring additional sensors or labelled fault data would help bridge this gap. Robust statistical processing is particularly attractive for this purpose because median and median absolute deviation (MAD) based methods have been demonstrated for adaptive thresholding in image-based structural-condition assessment [17]. In parallel, edge-based condition-monitoring systems have demonstrated the feasibility of implementing lightweight monitoring functions on embedded hardware [18]. These developments motivate the investigation of a statistically robust, low-complexity suspension monitoring approach.

This paper presents the Baseline-Normalized Suspension Degradation Index (SDI), which requires only a single accelerometer mounted on the chassis. As the damper wears, more vibration is transmitted near the resonance frequency of the sprung mass. The SDI quantifies this increase in vibration by comparing it with a healthy baseline constructed from the vehicle's recent driving history. The baseline is characterized using the median and the Median Absolute Deviation (MAD), two statistical measures that are less sensitive to isolated outliers and transient disturbances.

A hard pothole can produce vibration patterns similar to those caused by damper degradation. Relying only on the vibration signal may therefore result in a false alarm. To avoid this, the proposed SDI requires the fault indicator to remain above the threshold continuously for 15 s before it is identified as a genuine fault. This verification step is referred to as a persistence check. A second, independent check is provided by modelling the damper casing temperature. Damper wear increases heat generation, making the temperature signal sensitive to long-term degradation rather than isolated road events. Consequently, a single pothole does not produce a sustained thermal indication. The vibration and thermal channels are then combined through weighted decision fusion to produce a single Health Index. A fault is flagged when either individual channel or the fused Health Index exceeds its corresponding threshold.

The signal-processing techniques used in this work, including band-pass filtering, RMS envelope extraction, and MAD-based thresholding, are individually well established. The novelty lies in integrating these techniques with a self-referencing single-sensor framework, a persistence rule based on elapsed time rather than sample count, and a thermal channel driven by wear instead of vehicle operating duration. To the best of our knowledge, this integrated framework has not previously been tested and validated for suspension condition monitoring.

The main contributions of this work are summarized as follows. (1) A Baseline-Normalized SDI is formulated as a single-accelerometer, resonance-band vibration feature requiring no second sensor and

no labelled fault data. (2) A robust healthy baseline based on the median and median absolute deviation is developed to establish a distribution-free detection threshold. (3) A persistence criterion converts sample-level threshold crossings into time-calibrated fault confirmation. (4) A wear-dependent thermal model provides a complementary channel whose alarm is tied to accumulated degradation rather than to road-duration thermal inertia. (5) A weighted decision-fusion stage integrates the vibration and thermal channels into a bounded Health Index. (6) The proposed framework is validated using a quarter-car simulation with ISO 8608 road excitation, a transient pothole event, and programmed damping degradation. (7) Monte Carlo analysis over 25 road realizations, together with a parametric wear-sensitivity study, is conducted to characterize detection robustness and wear-specific thermal alarm behaviour. (8) Robustness is further evaluated across four road classes, four vehicle speeds, ±20% payload variation, and up to 5% sensor noise. Key algorithm parameters, including the threshold multiplier, persistence duration, and fusion weights, are justified through dedicated sensitivity analyses. In addition, the proposed SDI is compared with fixed-threshold and wavelet-energy benchmark methods using identical datasets.

The remainder of this paper is organized as follows. Section 2 contains the literature review; Section 3 presents the quarter-car model and the signal-processing framework underlying the proposed SDI. Section 4 reports the deterministic and statistical results. Section 5 discusses the practical implications and limitations of the proposed framework. Finally, Section 6 presents the conclusions.

2. Literature Review

Observer-based methods estimate suspension condition by comparing measured signals with a mathematical model of the system. Jeong and Choi generated suspension fault residuals using a quarter-car model and an unknown-input observer and subsequently classified the residuals using a support vector machine [1]. Reduced-order fault-detection filters have also been introduced for active suspension systems represented by Takagi–Sugeno fuzzy models, with the objective of maintaining robustness while reducing computational complexity [2]. More recently, an observer-based fault-detection strategy using a Takagi–Sugeno representation has been developed to estimate system states and fault signals while attenuating the influence of road disturbances [3]. These approaches provide valuable physical insight because the residual or estimated fault signal is directly related to the system model. However, their diagnostic performance depends on model fidelity and the ability of the model to represent variations in vehicle parameters and operating conditions.

Another class of approaches exploits suspension transmissibility and dynamic-response characteristics for damper diagnosis. Lozoya-Santos et al. proposed a fault-detection method for an automotive magnetorheological damper based on suspension transmissibility and road-frequency estimation [4]. Słomczyński et al. investigated a quarter-car suspension with a magnetorheological damper and modelled several suspension damage conditions within a backstepping-based control framework [5]. These studies demonstrate the usefulness of model-based dynamic characteristics for identifying suspension degradation and component damage. However, their approaches depend on suspension models and

system-specific information, which can limit direct application to low-complexity monitoring architectures.

Fault information can also be extracted directly from measured acceleration using time–frequency analysis. Early work applied wavelet transforms to detect faults in passive suspension systems [6]. Railway suspension degradation has also been investigated using wavelet-based features derived from lateral damper signals [7]. More recently, wavelet-based features have been combined with domain-adaptation techniques for suspension fault diagnosis under variable operating speeds [8]. These approaches are effective in capturing transient and frequency-dependent fault characteristics. However, time–frequency decomposition and feature extraction generally involve greater computational processing than a fixed-filter statistical approach, which may be relevant for low-cost embedded implementation.

Machine-learning classifiers provide another important class of suspension fault-diagnosis methods. Transfer learning has been applied to vibration-based suspension fault detection using radar-plot representations of vibration signals [9]. Decision-tree algorithms have been investigated for identifying multiple automobile suspension faults from vibration features [10]. A weightless neural network based on the WiSARD architecture has also been proposed for suspension fault diagnosis [11]. These methods demonstrate the ability of data-driven classifiers to distinguish different suspension fault conditions. However, their effectiveness depends on the availability of representative labelled data for the fault conditions and operating ranges considered. In addition, the computational and memory requirements associated with feature extraction and trained classifiers need to be considered when targeting resource-constrained embedded platforms.

Temperature-based monitoring provides a complementary means of assessing shock absorber condition. A patented monitoring device uses shock-absorber temperature measurements to determine a shock-wear condition and remaining useful life [12]. Howard et al. investigated monitoring the age of vehicle shock absorbers using cumulative work estimated through a calorimetry-based approach involving temperature measurements [13]. Experimental investigations have also examined temperature rise characteristics in valve-controlled adjustable damping shock absorbers [14]. The influence of temperature on hydraulic shock-absorber damping characteristics has been studied further [15], while Hryciów investigated the combined influence of temperature and technical condition on hydraulic shock absorber characteristics [16]. These studies establish the relevance of thermal information for suspension monitoring. However, the response of a simplified wear-dependent thermal model to random road excitation and short-duration disturbances remains comparatively less explored.

Robust statistical processing provides another avenue for low-complexity condition monitoring. Median and MAD-based processing has been demonstrated for adaptive thresholding in image-based concrete crack detection [17]. Although this application is outside the suspension domain, it demonstrates the usefulness of robust statistics when isolated disturbances or outliers are present. Edge-based condition monitoring has also been demonstrated for industrial equipment using low-cost transducers and embedded processing [18]. The latter study focused on pumping equipment and employed condition-monitoring and predictive-maintenance methods rather than the median/MAD approach used in the present work. Therefore, these studies provide supporting evidence for the broader feasibility of robust

statistical and embedded condition-monitoring architectures rather than direct evidence for suspension-specific MAD thresholding.

Road excitation is an important consideration when evaluating suspension degradation because the measured vehicle response depends strongly on the road input. ISO 8608 specifies a standardized approach for reporting measured road-surface profiles and provides a commonly used basis for generating stochastic road profiles for vibration studies [19]. Simulated road profiles based on ISO 8608 have been investigated for vibration analysis [20], while artificially generated profiles have also been used for road-roughness evaluation [21]. The use of standardized stochastic road excitation therefore provides a controlled basis for evaluating the robustness of suspension-monitoring algorithms under varying road realizations.

The literature indicates a clear trade-off among existing shock absorber condition-monitoring approaches. Model- and observer-based methods provide physically interpretable fault indicators but depend on model fidelity. Time–frequency approaches can capture detailed fault characteristics but may require greater computational processing. Machine-learning methods can distinguish multiple fault conditions but generally require labelled training data. Thermal methods provide an independent indication of accumulated damper behaviour but have been less extensively investigated under stochastic road excitation. Robust statistical methods offer a low-complexity alternative, but their application to single-sensor suspension degradation monitoring has received limited attention.

Accordingly, a gap remains for a single-sensor suspension-monitoring framework that evaluates damper condition relative to its own healthy operating history, does not require labelled fault data, and explicitly distinguishes persistent degradation from short-duration road disturbances. The influence of baseline construction, robust threshold selection, persistence duration, and complementary thermal information also warrants systematic evaluation. The proposed SDI framework addresses these aspects using a single chassis-mounted accelerometer, MAD-based baseline normalization, persistence-based fault confirmation, a wear-dependent thermal channel, and decision fusion.

Table 1: Comparison of shock absorber condition-monitoring approaches.

Method	Validation under Variable Road Conditions	Key limitation
Observer-based [1–3]	Performance depends on model accuracy	Accuracy tied to model fidelity
Transmissibility/model based [4,5]	Uses suspension dynamic characteristics for fault identification	Requires system-specific modelling and dynamic information
Vibration/time-frequency [6–8]	Effective for extracting fault-sensitive frequency/time-frequency features	Greater computational processing
Machine learning [9–11]	Effective classification of multiple fault conditions	Requires representative labelled data
Thermal [12–16]	Provides an independent indicator of damper condition	Behaviour under stochastic road excitation requires further study
Proposed SDI (this study)	Single-sensor, baseline-normalized monitoring with Monte Carlo evaluation	Experimental verification required

3. Mathematical Modelling and Fault Detection Framework

3.1 Quarter-Car Model

The suspension corner is modelled as a two-degree-of-freedom quarter-car with sprung mass m_s and unsprung mass m_u, coupled by spring stiffness k_s and a time-varying damper $c_s(t)$, with tire stiffness k_t and road displacement $z_r(t)$ as external input:

$$\mathrm{m_s} \cdot \ddot{\mathrm{z}}_\mathrm{s} + \mathrm{c_s(t)}(\dot{\mathrm{z}}_\mathrm{s} - \dot{\mathrm{z}}_\mathrm{u}) + \mathrm{k_s}(\mathrm{z_s} - \mathrm{z_u}) = 0 \quad (1)$$

$$\mathrm{m_u} \cdot \ddot{\mathrm{z}}_\mathrm{u} + \mathrm{c_s(t)}(\dot{\mathrm{z}}_\mathrm{u} - \dot{\mathrm{z}}_\mathrm{s}) + \mathrm{k_s}(\mathrm{z_u} - \mathrm{z_s}) + \mathrm{k_t}(\mathrm{z_u} - \mathrm{z_r}) = 0 \quad (2)$$

The state equations $X = [z_s, \dot{z}_s, z_u, \dot{z}_u]^T$ are integrated using a fixed-step fourth order Runge–Kutta solver with a sampling frequency of 100 Hz.

Table 2: Quarter car and road excitation parameters.

Symbol	Description	Value
m_s / m_u	Sprung / unsprung mass	350 / 45 kg
k_s/ k_t	Spring / tire stiffness	22,000 / 160,000 N/m
c_{s0} / $c_{s,final}$	Nominal / worn damping	1,500 / 450 N·s/m (30%)
$f_{n,sprung}$/ $f_{n,unsprung}$	Natural frequencies	1.262 / 9.490 Hz
Road class	ISO 8608	Class C
Vehicle speed	Constant	60 km/h (16.667 m/s)
Pothole	Raised-cosine pothole	60 mm / 0.5 s / t = 150 s
Wear window	Linear ramp	t = 200–500 s
f_s / duration	Sampling / run length	100 Hz / 500 s

3.2 Road Profile Generation and Pothole

The road profile is generated by spectral synthesis from the ISO 8608 spatial power spectral density

$$G_d(n) = G_d(n_0)(\frac{n}{n_0})^{-2} \quad (3)$$

with uniformly distributed random phase on each component, scaled to achieve a target RMS roughness of 6 mm. A raised-cosine pothole is superimposed:

$$z_{pot}(\tau) = -\frac{1}{2}D(1 - cos\, 2\pi\tau),\ \tau = (t - t_0)/T_p,\ t_0 \le t \le t_0 + T_p \quad (4)$$

with depth D = 60 mm, duration T_p = 0.5 s, and onset t_0 = 150 s.

3.3 Damper Wear Model

The damping coefficient decreases linearly from its nominal value c_{s0} to a terminal value $c_{s,final}$:

$$c_s(t) = \begin{cases} c_{s0}, t, & t \leq t_1 \\ c_{s0} + \alpha(c_{s,final} - c_{s0}), & t_1 < t < t_2 \\ c_{s,final}, & t \geq t_2 \end{cases} \quad (5)$$

where α = $(t - t_1)$ / $(t_2 - t_1)$, with t_1 = 200 s and t_2 = 500 s. The terminal value corresponds to 30% of nominal damping.

3.4 Suspension Degradation Index

The SDI is computed from the sprung-mass acceleration signal using a single accelerometer at each monitored suspension corner. The processing pipeline consists of six stages.

Stage 1: Band-pass filtering. A fourth-order Butterworth band-pass filter with a passband of 0.5–2.5 Hz is applied using zero-phase filtering to isolate the 1.262 Hz sprung-mass resonance.

Stage 2: Sliding RMS. A centred 5 s (500-sample) window computes the instantaneous vibration energy, with edge replication applied at the signal boundaries.

Stage 3: Median filtering. An 11-sample median filter suppresses isolated impulsive disturbances while preserving the underlying trend.

Stage 4: Moving-average smoothing. A 2 s (200-sample) moving-average filter generates the final vibration envelope, $v_{\mathrm{rms,smooth}}(t)$.

Stage 5: Baseline normalization. The median of $v_{\mathrm{rms,smooth}}$ during the healthy operating period ($t \leq 150$ s) is used as the baseline $\tilde{b}$. The SDI is defined as:

$$SDI(t) = \frac{v_{rms,smooth}(t)}{\tilde{b}} \quad (6)$$

so that the SDI is approximately one during healthy operation and increases as damper degradation progresses.

Stage 6: Robust thresholding. The detection threshold is determined from the median absolute deviation (MAD) of the healthy baseline:

$$MAD = median(|v_{rms,smooth,baseline} - \tilde{b}|) \quad (7)$$

$$\tau = 1 + k \cdot (\frac{MAD}{\tilde{b}}),\ k = 2.2 \quad (8)$$

The median and MAD are adopted instead of the mean and standard deviation because they are less sensitive to isolated outliers, providing a more stable baseline for long-term monitoring. The value k =2.2 was selected through a parameter sensitivity analysis presented in Section 4.8, providing a balance between early fault detection and false-alarm rejection.

3.5 Persistence-Based Fault Confirmation

The SDI is converted into a fault decision by threshold comparison followed by persistence verification. At each sample, a counter increments while SDI(k) > τ and resets to zero otherwise. A fault is confirmed only when the counter reaches the required number of consecutive samples:

$$N_{required} = P_{persistence} \times f_s \tag{9}$$

$$= 15 \times 100 = 1500\, samples$$

corresponding to 15 s of continuous threshold exceedance. This persistence criterion prevents short-duration transient events, such as pothole impacts, from producing false alarms while allowing sustained changes associated with progressive damper degradation to be detected. Once confirmed, the fault flag remains latched for the rest of the monitoring period.

The overall fault decision combines the SDI-based fault flag with the thermal alarm (Section 3.6) using a logical OR operation. The persistence duration of 15 s was selected through the parameter sensitivity analysis presented in Section 4.8, providing a conservative balance between transient rejection and reliable fault detection.

3.6 Wear-Dependent Thermal Model

A first-order lumped-parameter thermal model is used to estimate the damper casing temperature:

$$C_{th} \cdot \dot{\theta} = P_0 + c_s(t)(\dot{z}_s - \dot{z}_u)^2 + P_{wear} - h(\theta - \theta_{amb}) \tag{10}$$

where the initial temperature is $\theta(0) = \theta_{\mathrm{amb}} = 25^{\circ}\mathrm{C}$, the thermal capacitance is $C_{\mathrm{th}} = 60\ \mathrm{J/K}$, the heat-loss coefficient is $h = 1.0\ \mathrm{W/K}$, and the baseline heat input is $P_0 = 4\ \mathrm{W}$.

The wear-dependent heat generation is defined as

$$P_{wear} = C_{extra} \cdot w(t) \tag{11}$$

$$w(t) = \left(1 - \frac{c_s(t)}{c_{s0}}\right) \tag{12}$$

where $C_{\mathrm{extra}} = 35$ and $w(t)$ is the instantaneous wear fraction. The wear fraction is zero before the onset of degradation and increases linearly as the damping coefficient decreases. The additional heat generation is directly related to damper wear, enabling the thermal model to distinguish progressive degradation from normal operating conditions. A thermal alarm is generated when the estimated temperature exceeds the alarm threshold of 40°C.

The signal-processing, thermal-model, and decision-fusion parameters used throughout the proposed framework are summarized in Table 3.

Table 3: Signal processing, thermal, and decision-fusion parameters.

Signal-processing	Value	Thermal model	Value
Filter order / passband	4 / 0.5-2.5 Hz	Ambient temperature	25°C
Sliding RMS window	5 s (500 samples)	Thermal capacitance, C_{th}	60 J/K
Median filter length	11 samples	Heat-loss coefficient, h	1.0 W/K
Moving-average length	2 s (200 samples)	Baseline power, P_0	4 W
Baseline heat input	t ≤ 150 s	Wear-heating coefficient, C_{extra}	35
MAD multiplier k	2.2	Thermal alarm threshold	40°C
Persistence duration	15 s (1500 samples)	Fusion weights (SDI/Thermal)	0.70 / 0.30
Monte Carlo trials	25	Fusion alarm threshold	0.70

3.7 Decision Fusion

The SDI and temperature are normalized with respect to their corresponding alarm thresholds. Each quantity is limited to twice its alarm reference and scaled to the interval [0,1]:

$$SDI_{norm} = \frac{min(SDI/\tau,2)}{2} \quad (13)$$

$$Temp_{norm} = \frac{min(\theta/\theta_{alarm},2)}{2} \quad (14)$$

The normalized quantities are combined to obtain the Health Index (HI):

$$HI(t) = \min\left[1, w_{SDI} \cdot SDI_{norm}(t) + w_{Temp} \cdot Temp_{norm}(t)\right] \quad (15)$$

where

$w_{SDI} = 0.70,\ w_{Temp} = 0.30, \qquad w_{SDI} + w_{Temp} = 1,$

A suspension fault is declared when HI ≥ 0.70. The weighting factors of 0.70 for the SDI and 0.30 for the thermal channel were selected through the parameter sensitivity analysis presented in Section 4.8. This combination provides a balanced contribution from both monitoring channels while maintaining reliable fault detection.

3.8 Monte Carlo Validation

The proposed monitoring framework was evaluated using 25 independent road realizations (random seeds 2-26). For each trial, all vehicle, degradation, and monitoring parameters were kept unchanged, while only the road profile was varied to assess the influence of road-profile variability on diagnostic performance. The recorded performance metrics include the fault detection time, peak SDI, peak damper temperature, peak Health Index, and fault detection status.

4. Results

The proposed SDI was evaluated using a deterministic baseline scenario and a series of parametric studies. The baseline simulation used random seed 1 with an ISO 8608 Class-C road profile at a vehicle speed of 60 km/h. The pothole and wear-ramp parameters are listed in Table 2. The signal-processing and thermal parameters are listed in Table 3. The evaluation was subsequently extended through wear-sensitivity, robustness, parameter-sensitivity, and benchmark studies, as presented in Sections 4.6–4.9.

4.1 Road Excitation and Vehicle Response

The quarter-car model was excited using an ISO 8608 Class-C road profile with an embedded pothole. Figure 1 shows the generated road profile used throughout the baseline simulation. Away from the pothole, the profile follows the random characteristics of a Class-C road, while the embedded 60 mm pothole provides the primary transient disturbance for evaluating the suspension response.

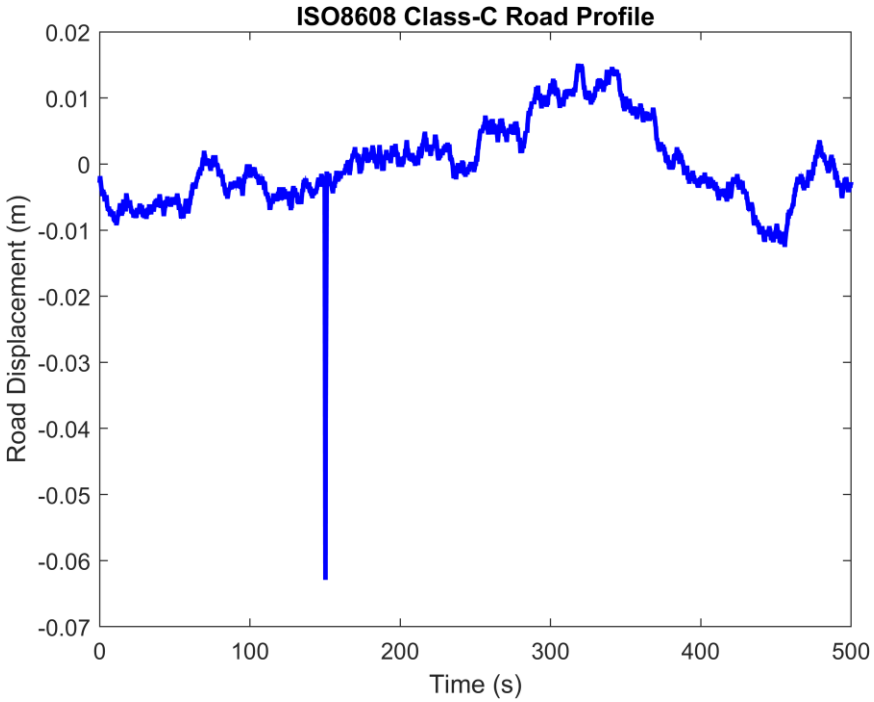


Figure 1: ISO 8608 Class-C road profile used in the baseline simulation.

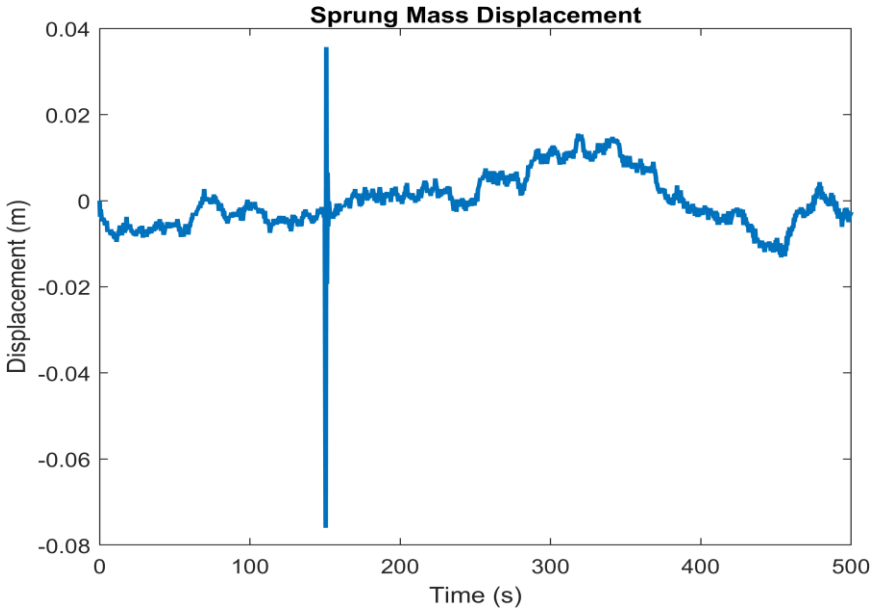


Figure 2: Sprung-mass displacement response.

The sprung-mass displacement and acceleration responses of the quarter-car model are shown in Figures 2 and 3. In both signals, the pothole transient dominates the response, whereas the influence of progressive damper wear remains comparatively small because of the relatively low roughness of the Class-C road. These observations highlight the difficulty of detecting gradual suspension degradation directly from raw vehicle responses. Figure 4 illustrates the prescribed damper wear profile used throughout the simulation. The damping coefficient is maintained at 1500 N·s/m until 200 s and then decreases linearly to 450 N·s/m by 500 s, representing progressive degradation to 30% of its nominal value. This wear profile provides the reference degradation scenario used for evaluating the proposed Suspension Degradation Index (SDI).

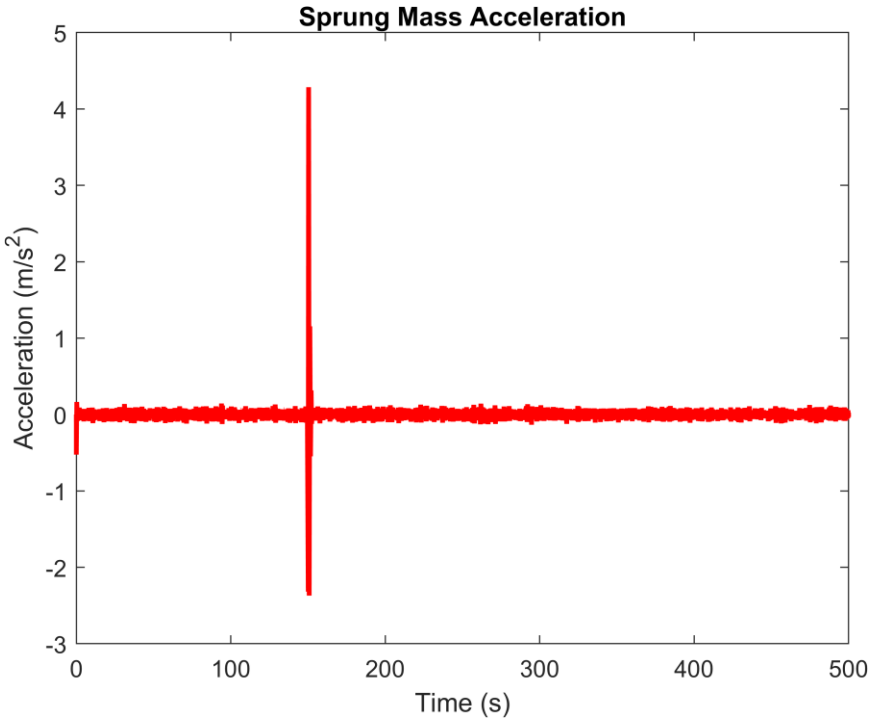


Figure 3: Sprung-mass acceleration response.

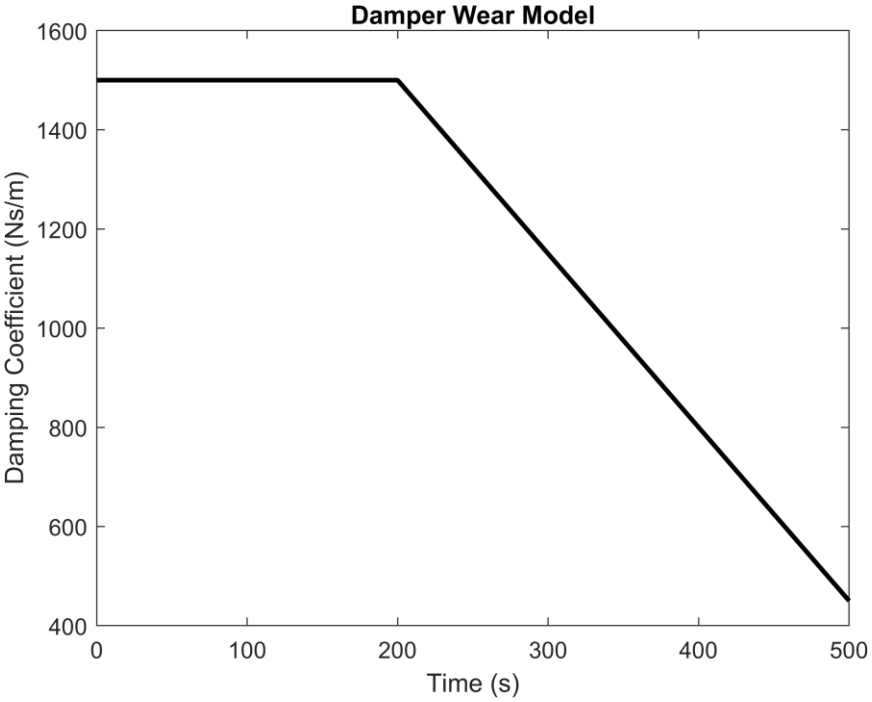


Figure 4: Damper wear profile.

4.2 SDI Channel and Fault Detection

The sprung-mass acceleration was filtered using a 0.5–2.5 Hz band-pass filter to isolate the suspension resonance band most sensitive to changes in damping. Figure 5 shows the filtered signal, in which the

pothole produces the dominant transient response, while the remaining signal contains the lower-amplitude vibration used for degradation analysis. Figure 6 illustrates the successive stages of the sliding-RMS processing. The raw, median-filtered, and smoothed RMS signals closely overlap throughout the simulation, indicating that the filtering procedure preserves the underlying vibration trend while effectively suppressing isolated fluctuations. The healthy operating period was used to establish the baseline statistics, yielding a median RMS of 0.02097 m/s², a median absolute deviation (MAD) of 0.002772 m/s², and a detection threshold of 1.2908.

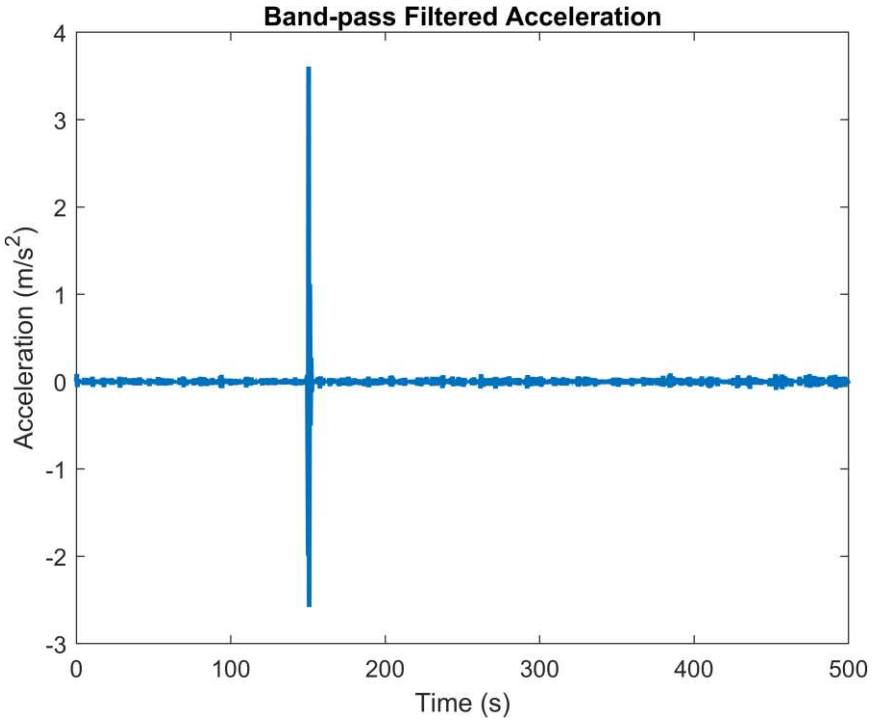


Figure 5: Band-pass filtered sprung-mass acceleration (0.5–2.5 Hz).

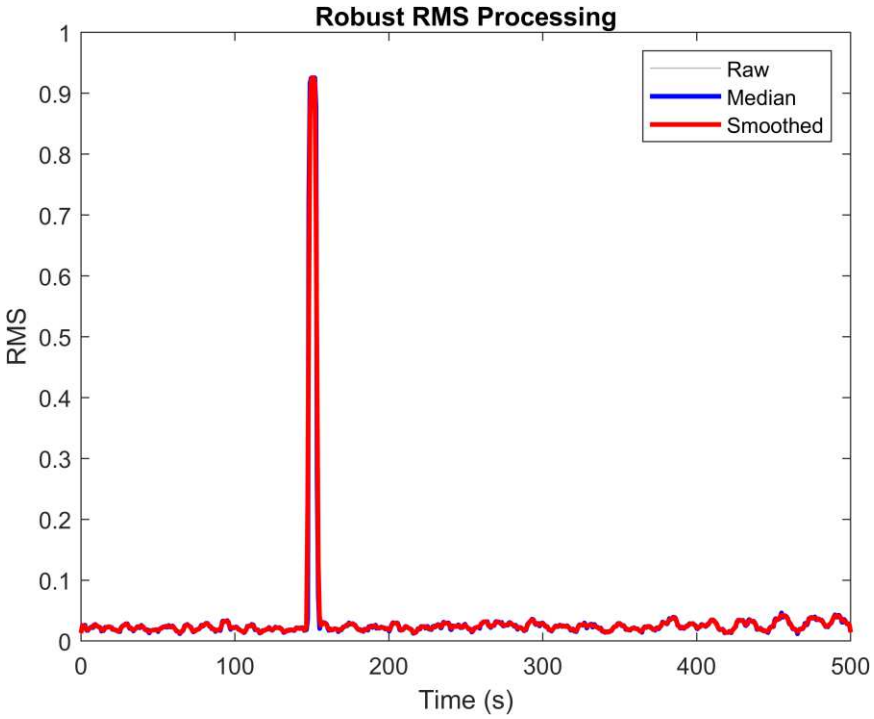


Figure 6: Sliding-RMS processing of the filtered acceleration.

Figure 7 presents the Suspension Degradation Index (SDI) over the entire 500 s simulation. The pothole produces the largest SDI peak (44.15) at approximately 150 s, whereas the SDI remains close to unity during healthy operation. As damper wear progresses, the baseline SDI gradually increases, indicating increasing vibration energy within the resonance band. This gradual upward trend demonstrates that the proposed SDI is sensitive to progressive damping degradation while remaining robust to normal road-induced excitation. Table 4 further quantify this behaviour by dividing the wear period into successive time intervals. The mean SDI increases from 1.10 during the early wear stage to 1.50 during the late wear stage, while the percentage of samples exceeding the detection threshold rises from 15.9% to 72.0%. These results confirm that the proposed SDI consistently tracks progressive damping loss.

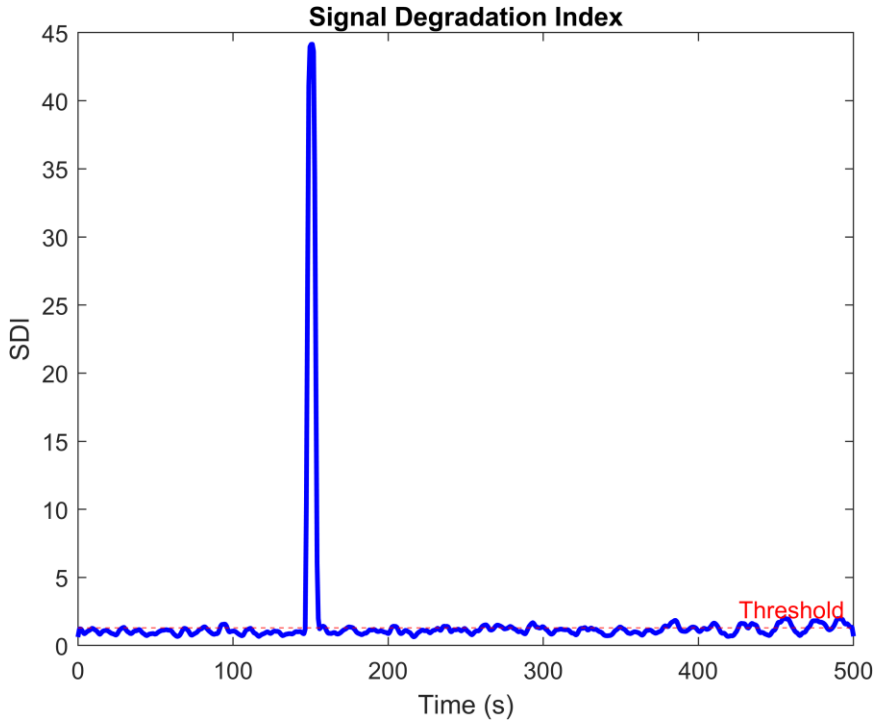


Figure 7: Suspension Degradation Index (SDI).

Table 4: SDI statistics for different stages of the simulation.

Interval	Mean SDI	Maximum SDI	Samples > τ (%)
0-150 s (healthy)	1.01*	44.10*	8.0%
150-152 s (pothole)	44.07	44.15	100%
200-250 s (early wear)	1.10	1.42	15.9%
250-300 s	1.24	1.68	45.2%
300-350 s	1.06	1.37	6.8%
350-400 s	1.17	1.84	28.9%
400-450 s	1.16	1.65	35.4%
450-500 s (late wear)	1.50	2.03	72.0%

*The healthy interval includes residual effects of the pothole due to the 2 s smoothing window.

The persistence counter used for fault declaration is shown in Figure 8. A fault is declared only when the SDI remains above the detection threshold for 1500 consecutive samples (15 s). Although the pothole produces a large transient response, the persistence counter increases to only about 200 samples, well below the required persistence interval. During the progressive wear phase, the counter reaches a maximum of 1270 samples at approximately 499 s, but still does not satisfy the 15 s persistence criterion. Consequently, no SDI-based fault is declared for this deterministic simulation, demonstrating that the persistence logic effectively rejects short-duration transients and intermittent threshold crossings caused by normal Class-C road excitation.

The effectiveness of the persistence criterion is further validated through the Monte Carlo study presented in Section 4.5, where 19 of 25 simulation runs achieve sustained threshold exceedance and successfully trigger fault detection as damper degradation progresses.

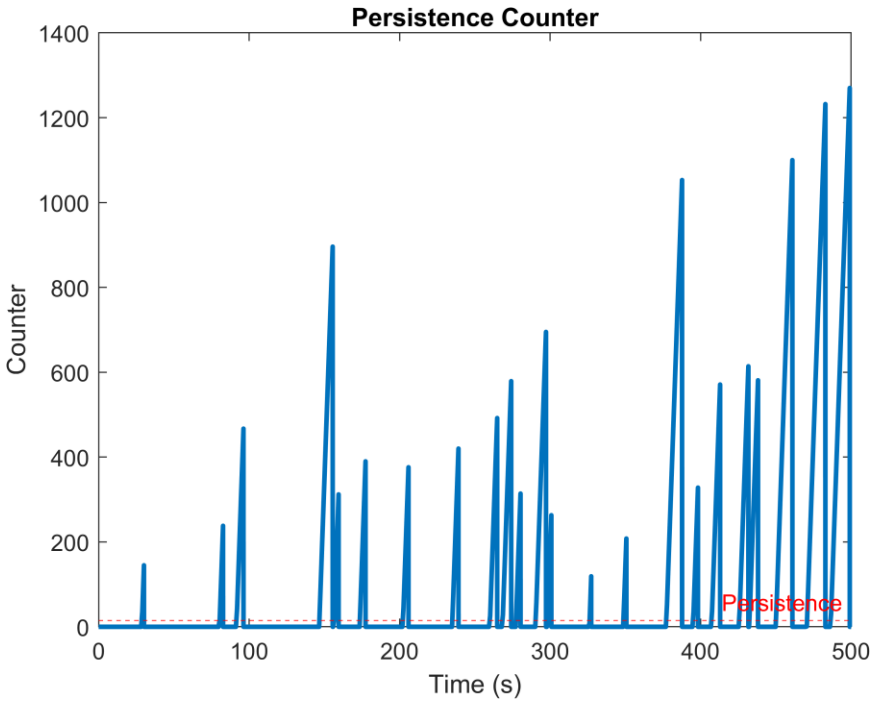


Figure 8: Persistence counter for SDI threshold exceedances.

4.3 Thermal Monitoring

Figure 9 shows the instantaneous damper power dissipation, while Figure 10 presents the corresponding estimated damper casing temperature. During healthy operation, the temperature rises gradually from the ambient value of 25°C and approaches a steady-state value of approximately 29°C, remaining well below the 40°C alarm threshold. After damper degradation begins at 200 s, the wear-dependent power increases progressively, producing a corresponding rise in the estimated casing temperature. The temperature exceeds the alarm threshold at 391.04 s, when the damping coefficient has decreased to approximately 858 N·s/m (57% of its nominal value), and reaches a maximum of 48.70°C at the end of the simulation. Although the pothole generates a large instantaneous power spike (373.8 W) in Figure 9, it produces only a small temperature fluctuation because of the thermal inertia of the damper. These results demonstrate that the proposed thermal monitoring channel responds primarily to sustained wear-induced heating rather than to isolated transient excitation.

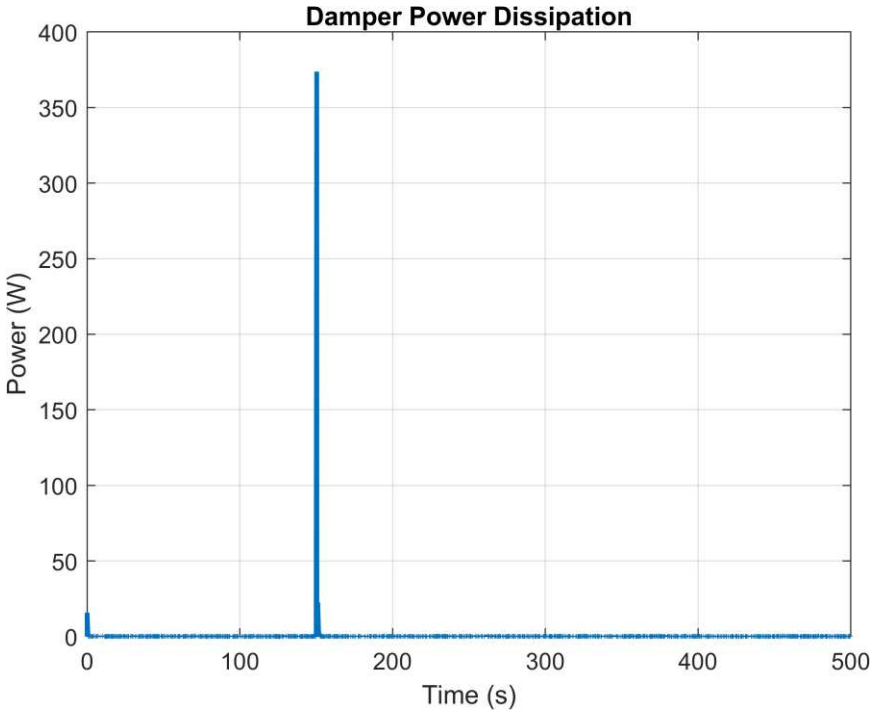


Figure 9: Instantaneous damper power dissipation.

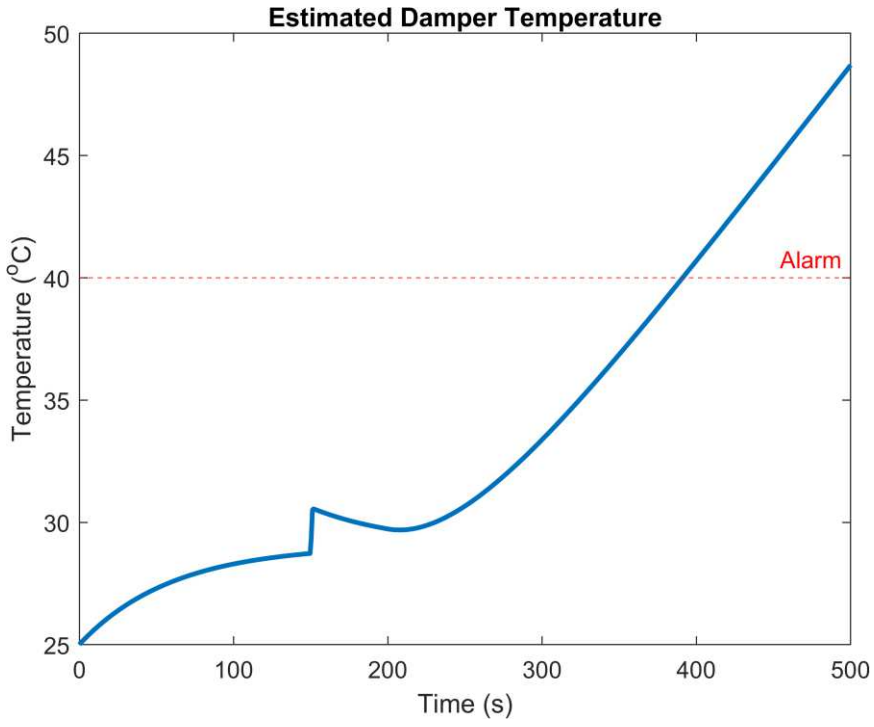


Figure 10: Estimated damper casing temperature with the alarm threshold.

4.4 Decision Fusion

During healthy operation, the health index remains well below the alarm threshold. Figure 11 shows the decision fusion health index obtained by combining the SDI and thermal monitoring channels. The pothole

produces a short-duration transient, whereas progressive damper degradation causes a gradual increase in the health index during the wear period.

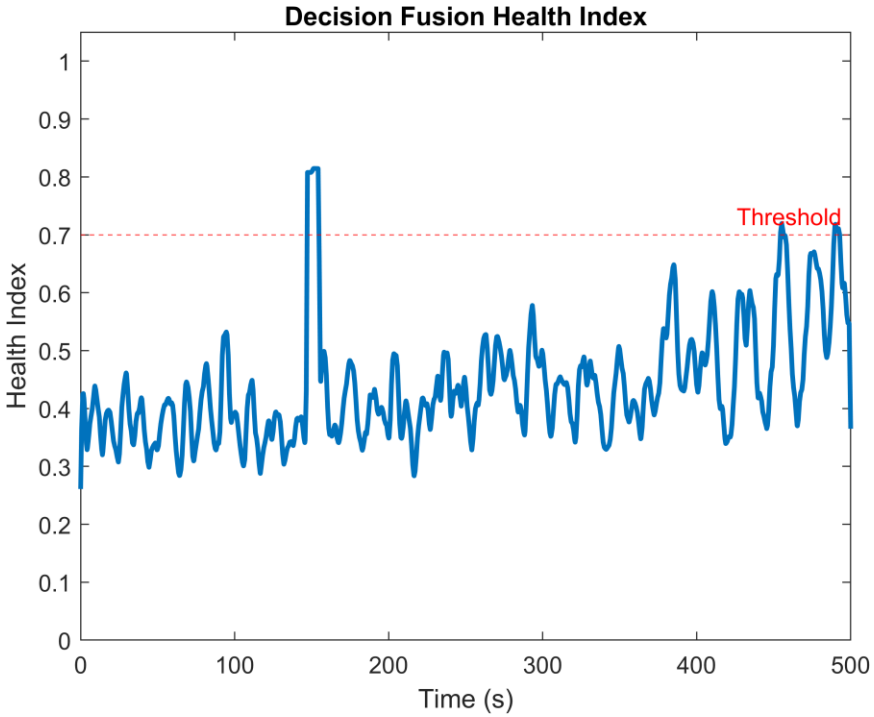


Figure 11: Decision fusion health index with the alarm threshold.

The overall system declares fault detected, driven primarily by the thermal alarm, while the SDI and fusion channels provide complementary evidence of progressive degradation. Table 5 summarizes the principal numerical results obtained from the deterministic baseline simulation.

Table 5: Summary of key performance metrics for the deterministic baseline simulation.

Performance Metric	**Result**
Baseline SDI statistics (Median / MAD / Threshold)	0.02097 m/s² / 0.002772 m/s² / 1.2908
Maximum SDI	44.147 (pothole, t ≈ 150 s)
Maximum persistence counter	1270 samples (12.7 s)
SDI persistence	Not triggered (1270 < 1500 samples required)
Thermal alarm time	t = 391.04 s
Maximum damper temperature	48.70°C
Maximum damper power	373.8 W (pothole event)
Fusion first alarm	t = 146.71 s (pothole transient)
Maximum Health Index (full run / wear period)	0.815 / 0.719
Overall system decision	Fault detected (thermal alarm)

4.5 Monte Carlo Validation

A 25-trial Monte Carlo study was conducted by varying only the random seed used for road generation while keeping the vehicle speed, pothole profile, and wear progression unchanged. The proposed monitoring framework achieved a 100% detection rate across all 25 Monte Carlo trials.

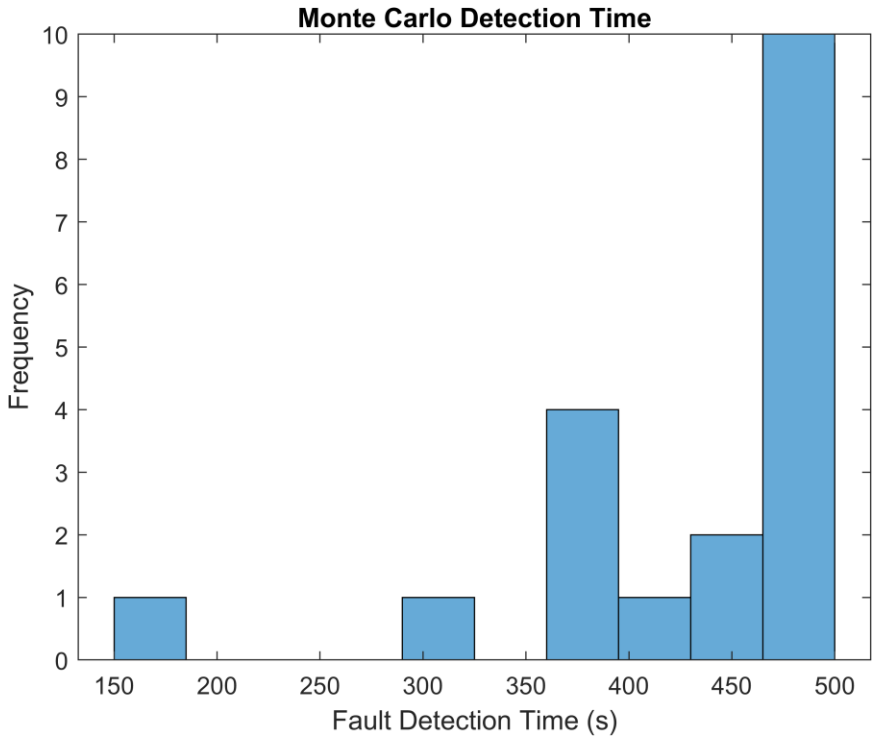


Figure 12: Distribution of Monte Carlo fault-detection times across 25 trials.

The SDI-persistence channel successfully detected progressive damper degradation in 19 of 25 trials (76%), with a mean detection time of 425 s. Detection events were concentrated between 370 s and 493 s, corresponding to the later stages of the wear process. In the remaining six trials, the persistence counter approached, but did not reach, the required 1500-sample threshold. Nevertheless, these trials were successfully detected by the thermal monitoring channel, resulting in a 100% overall detection rate. Table 6 summarizes the principal statistics obtained from the Monte Carlo study.

Table 6: Summary statistics for the 25 Monte Carlo trials.

Performance Metric	Mean ± SD	Minimum	Maximum
SDI persistence fault time (s)	425.1 ± 80.4 (19/25 trials)	155.6	493.0
Maximum temperature (°C)	48.70 ± 0.002	48.70	48.70
Maximum SDI	44.18 ± 1.79	41.94	49.13
Maximum Health Index	0.844 ± 0.028	0.815	0.882
Overall detection rate	100%	—	—

Figures 13 to 15 summarize the variability of the principal fault detection indicators across the 25 Monte

Carlo trials. The maximum damper temperature exhibits negligible variation because the thermal model is governed primarily by the deterministic wear profile. In contrast, the maximum SDI and Health Index vary across trials owing to differences in the stochastic road realization, although all values remain within a narrow range, demonstrating the robustness of the proposed monitoring framework.

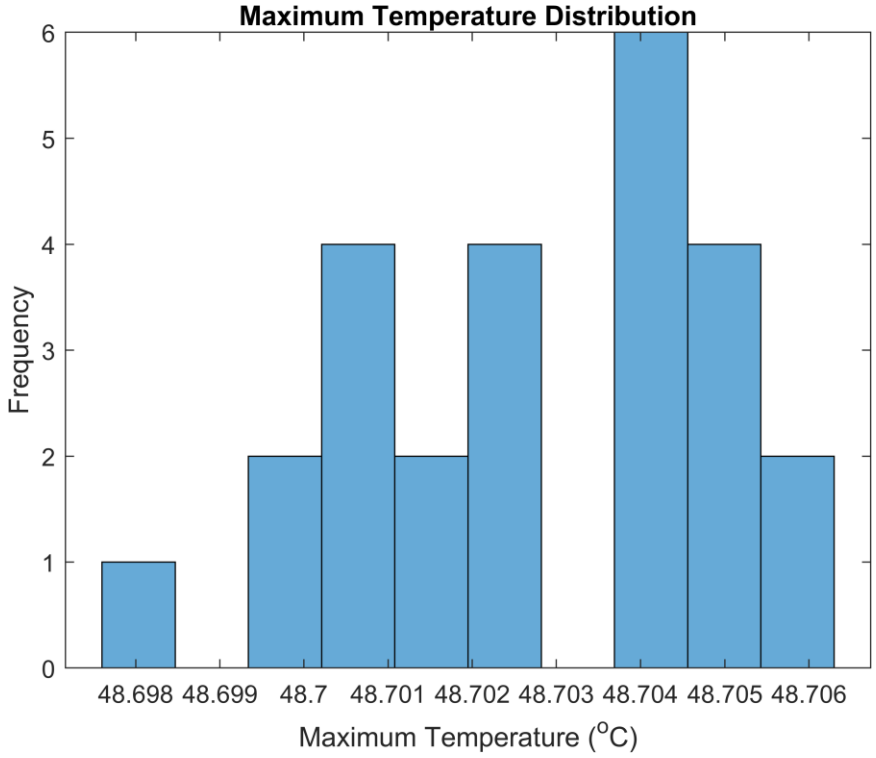


Figure 13: Distribution of Monte Carlo maximum damper temperature.

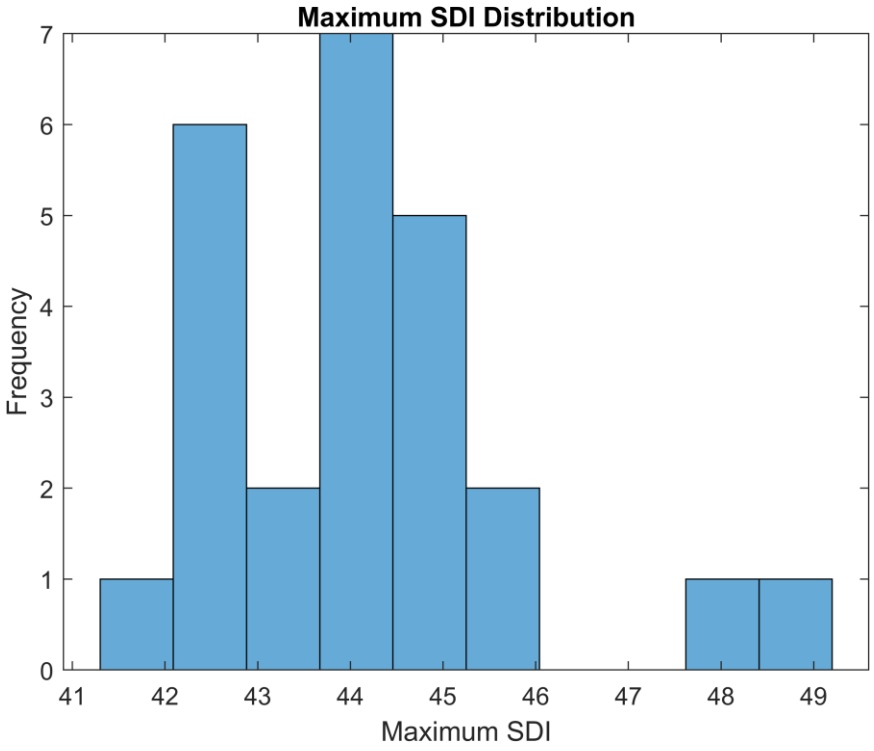


Figure 14: Distribution of Monte Carlo maximum SDI.

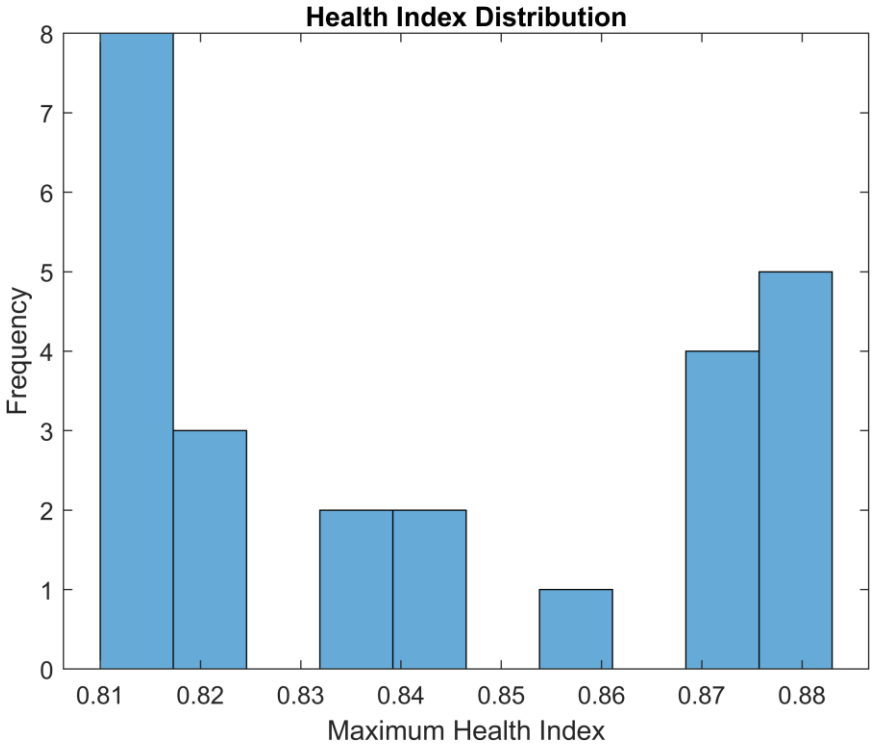


Figure 15: Distribution of Monte Carlo maximum Health Index.

4.6 Thermal Wear-Sensitivity Analysis

A parametric wear-sensitivity study was conducted to evaluate the thermal alarm response over wear levels ranging from 0% to 70% of the nominal damping coefficient. Table 7 summarizes the corresponding thermal response. The thermal alarm is first activated at approximately 40% wear (900 N·s/m), when the estimated temperature exceeds the 40°C alarm threshold. The maximum damper temperature increases from 30.5°C under healthy conditions to 48.7°C at 70% wear, indicating an approximately linear increase with progressive degradation. These results confirm that the proposed thermal monitoring channel responds consistently to accumulated damper wear while avoiding false alarms under healthy operating conditions and at all tested wear levels below 40%.

Table 7: Thermal response as a function of damper wear.

Wear (%)	Final damping coefficient (N·s/m)	Maximum temperature (°C)	Thermal alarm
0 (Healthy)	1500	30.5	No
10	1350	31.9	No
20	1200	34.7	No
30	1050	37.5	No
40	900	40.3	Yes
50	750	43.1	Yes
60	600	45.9	Yes
70 (reference case)	450	48.7	Yes

4.7 Robustness Analysis

The robustness of the proposed framework was evaluated across four ISO 8608 road classes (A–D), four vehicle speeds (40–100 km/h), five payload levels (±20% of the nominal sprung mass), and three sensor-noise levels (0%, 2%, and 5% of the healthy-period acceleration RMS).

Table 8: Detection performance under different road classes and vehicle speeds.

Road class	Maximum SDI	SDI detections	Thermal alarm time (s)	Overall fault detections
A	42.18–45.01	1 / 4	391.03–391.11	4 / 4
B	43.34–46.50	3 / 4	391.06–391.09	4 / 4
C	43.23–45.78	4 / 4	391.05–391.11	4 / 4
D	40.10–44.52	3 / 4	391.05–391.11	4 / 4

The thermal alarm is triggered within a narrow interval (391.03–391.11 s) for all 16 road class and vehicle speed combinations, resulting in a 100% overall fault detection rate, as summarized in Table 8. The SDI channel independently detects the fault in 11 of the 16 operating conditions (69%), while the remaining cases are successfully identified by the thermal monitoring channel. Since all simulated road profiles were

normalized to the same 6 mm RMS roughness (Section 3.2), no systematic dependence on road class is observed. The reported results therefore reflect the adopted road-generation methodology rather than the inherent effect of ISO 8608 road severity.

Table 9: Detection performance under payload variation.

Payload factor	Sprung mass (kg)	Maximum SDI	SDI fault time (s)	Thermal alarm time (s)
0.8×	280	45.73	273.93	391.06
0.9×	315	45.00	484.59	391.04
1.0× (Nominal)	350	44.15	Not triggered	391.04
1.1×	385	43.70	Not triggered	391.04
1.2×	420	43.71	463.84	391.04

Furthermore, the thermal alarm time remains nearly constant (391.04–391.06 s) for all payload levels, indicating that the thermal monitoring channel is insensitive to payload variation, as shown in Table 9. The SDI channel detects the fault at the two lightest payloads and the heaviest payload, but not at the nominal or 1.1× nominal payload for this realization, owing to changes in the sprung-mass dynamic response. Despite this variation, the proposed decision-fusion framework achieves a 100% overall fault detection rate through the thermal monitoring channel.

Table 10: Detection performance under different sensor-noise levels.

Noise level	Maximum SDI	Baseline false-positive rate (%)	SDI fault time (s)
0% (Clean)	44.15	7.97	Not triggered
2%	44.14	7.90	Not triggered
5%	44.19	7.94	Not triggered

The maximum SDI and the baseline false-positive rate show negligible variation under sensor-noise levels of up to 5% of the healthy-period acceleration RMS, as listed in Table 10. The SDI persistence criterion is not met for any of the tested noise levels. However, the proposed decision-fusion framework maintains a 100% overall fault detection rate through the thermal monitoring channel.

4.8 Parameter Sensitivity

A sensitivity analysis was performed to evaluate the selected values of the MAD multiplier (k), persistence duration, and fusion weights described in Sections 3.4, 3.5, and 3.7. The baseline false-positive rate decreases as the MAD multiplier increases because of the higher detection threshold as shown in Table 11. A value of k = 2.2 was selected as a compromise between detection sensitivity and false-alarm rejection.

Table 11: Effect of the MAD multiplier (k) on the baseline false-positive rate.

MAD multiplier (k)	Detection threshold (τ)	Baseline false-positive rate (%)
1.5	1.198	15.9
1.8	1.238	11.8
2.0	1.264	8.8
2.2 (Selected)	**1.291**	**8.0**
2.5	1.330	6.6
3.0	1.397	5.0

Table 12 indicates that the persistence duration strongly influences SDI fault detection. A value of 15 s was selected because shorter durations respond to pothole transients, whereas longer durations suppress SDI detection.

Table 12: Effect of persistence duration on SDI fault detection.

Persistence duration (s)	Required samples	SDI fault detection
5	500	151.55 s (pothole-adjacent)
10	1000	387.13 s (wear-driven)
15 (Selected)	**1500**	**Not triggered (thermal backup)**
20	2000	Not triggered (thermal backup)
30	3000	Not triggered (thermal backup)

Increasing the SDI weight increases the maximum Health Index and advances the fusion alarm time, as shown in Table 13. The selected weighting (0.7/0.3) provides a balance between responsiveness and robustness while maintaining reliable fault detection during the wear period.

Table 13: Effect of fusion weights on Health Index performance.

SDI weight / Thermal weight	Maximum Health Index	Fusion alarm time(s)	Maximum Health Index during wear
0.5 / 0.5	0.691	Not triggered	0.684
0.6 / 0.4	0.753	146.74	0.701
0.7 / 0.3 (Selected)	**0.815**	**146.71**	**0.719**
0.8 / 0.2	0.876	146.69	0.742
0.9 / 0.1	0.938	146.67	0.764

4.9 Benchmark Comparison

The proposed SDI was compared with two baseline methods evaluated using the same deterministic simulation: (i) a fixed RMS threshold (mean + 3σ) applied to the unfiltered sliding-window RMS acceleration and (ii) a wavelet band-energy feature computed over the 0.5–2.5 Hz frequency band. Both methods employed the same 15 s persistence criterion as the proposed SDI.

Table 14: Benchmark comparison on the deterministic baseline run.

Method	Fault detection	Baseline false-positive rate (%)
Fixed RMS threshold (3σ)	Not triggered	1.47%
Wavelet band energy (3σ)	Not triggered	1.54%
Proposed SDI (k = 2.2)	Not triggered	7.97%

Neither the fixed RMS threshold nor the wavelet band-energy method satisfies the persistence criterion during the baseline simulation, resulting in no confirmed fault detection, as shown in Table 14. Although both baseline methods exhibit lower baseline false-positive rates than the proposed SDI, they also fail to detect progressive damper degradation. The proposed fault-detection framework combines the SDI with thermal monitoring through decision fusion, maintaining a 100% overall fault detection rate under the baseline simulation.

5. Discussion

5.1 Discussion of SDI Performance

The baseline-normalized SDI reflects the increase in sprung-mass vibration caused by progressive damping loss within the suspension resonance band. As damper wear increases, both the mean SDI and the percentage of samples exceeding the threshold increase (Table 4), reflecting the higher resonance response associated with a lower damping ratio. The selected 0.5-2.5 Hz passband isolates this behaviour, making the SDI sensitive to changes in suspension dynamics rather than broadband vibration.

The 15 s persistence criterion distinguishes short-duration road disturbances from progressive damper degradation. Although the pothole event produces a large instantaneous SDI, the exceedance duration is insufficient to satisfy the persistence requirement. In contrast, progressive wear produces sustained threshold exceedance in 19 of the 25 Monte Carlo trials, indicating that the SDI responds to persistent changes in vibration behaviour rather than isolated transient events.

5.2 Thermal Channel

The wear-dependent thermal model generates a deterministic alarm linked to accumulated damper degradation through the additional wear-induced heating term, $P_{\mathrm{wear}} = C_{\mathrm{extra}}\, w(t)$. Under healthy conditions, the steady-state temperature remains below the 40°C alarm threshold. As wear progresses, the additional heat generation increases the damper temperature, and the thermal alarm is activated at approximately 40% wear. The activation point can be adjusted by modifying either C_{extra}or the alarm threshold $\theta_{\mathrm{alarm}}$to suit different application requirements.

The SDI and thermal channels provide complementary information. The SDI reflects changes in vibration behaviour and its detection depends on the excitation produced by a particular road realization. In contrast, the thermal channel follows the deterministic wear trajectory and produces a consistent alarm

independent of road conditions. Combining the two channels through OR decision fusion achieves a 100% fault detection rate while reducing the likelihood of missed detections.

The proposed framework requires only a single chassis-mounted accelerometer and a simple thermal model. Unlike existing approaches, it does not rely on complex models or data-driven training, making it suitable for real-time implementation. The proposed algorithm combines fixed-coefficient filtering with simple statistical analysis, resulting in low computational complexity. The thermal channel complements the vibration-based SDI by providing an independent indication of damper degradation.

5.3 Robustness and Benchmark Discussion

The robustness analysis shows that the overall fault detection performance is maintained across the investigated road classes, vehicle speeds, payloads, and sensor-noise levels. This behaviour is primarily due to the thermal channel, which depends only on the wear trajectory and is independent of road excitation. As a result, the overall decision-fusion framework does not require retuning across the operating conditions evaluated. The road-class analysis, however, should be interpreted in the context of the adopted road-generation method. Since all ISO 8608 road classes were normalized to the same 6 mm RMS value, the comparison mainly reflects differences in road realization and vehicle speed rather than variations in road roughness severity.

The payload analysis highlights the complementary roles of the SDI and thermal channels. The SDI response varies with the sprung mass because changes in vehicle mass shift the suspension resonance frequency relative to the fixed 0.5–2.5 Hz analysis band. In contrast, the thermal channel is unaffected by payload variation and provides a consistent fault indication. A payload-adaptive frequency band could further improve the robustness of the SDI under a wider range of loading conditions.

The benchmark comparison shows that the proposed SDI produces a higher baseline false-positive rate than the fixed RMS threshold and wavelet band-energy methods. This behaviour results from the selected $k = 2.2$ threshold, which favours detection sensitivity over conservative thresholding. Despite this difference, none of the three vibration-based methods produces a persistence-confirmed fault during the deterministic baseline simulation. The principal advantage of the framework lies in the integration of vibration and temperature-based information through decision fusion. The thermal channel provides an independent confirmation of progressive damper degradation, enabling the overall framework to achieve 100% fault detection in all evaluated scenarios.

5.4 Computational Complexity and Embedded Feasibility

The proposed algorithm has $O(N)$ time complexity over an N-sample record and requires only $O(1)$ additional memory apart from a small number of rolling buffers. The computation is based on fixed-coefficient filtering, sliding-window statistics, median filtering, persistence logic, and a first-order thermal model, all of which operate with constant computational effort per sample. Consequently, the computational cost scales linearly with the length of the input signal while maintaining a small memory footprint.

Unlike wavelet-based [6–8] and machine-learning-based [9–11] methods, the proposed framework does not require iterative optimization, matrix computations, or trained model parameters. These characteristics make the algorithm suitable for real-time embedded implementation. The computational complexity discussed here is based on the algorithmic structure rather than execution time measurements. Performance profiling on a target embedded platform remains part of future work.

5.5 Limitations and Future Work

This work is validated through simulation using a quarter-car model with synthesized ISO 8608 road profiles and a controlled linear damper degradation profile. The proposed model does not consider full-vehicle dynamics, such as pitch, roll, steering, or multi-wheel interactions, and the thermal model is based on a simplified first-order representation of damper heating. The benchmark comparison is limited to a deterministic simulation, and the computational complexity analysis is based on algorithmic complexity rather than execution-time measurements on embedded hardware. These assumptions provide a controlled environment for evaluating the proposed fault-detection framework but should be considered when extending the approach to practical vehicle applications.

Future work will focus on experimental validation using an instrumented suspension test rig or an in-vehicle platform, together with execution-time profiling on embedded hardware. Additional studies will investigate full-vehicle modelling, road-generation methods that preserve ISO 8608 class-dependent roughness severity, benchmark evaluation across multiple road realizations, and alternative decision-fusion strategies, including Bayesian and evidence-based fusion. Extending the framework to nonlinear damper degradation mechanisms and real-world operating conditions will further improve its practical applicability.

6. Conclusions

A suspension health-monitoring framework based on a baseline-normalized Suspension Degradation Index (SDI) and a wear-dependent thermal model has been developed and validated using a quarter-car simulation model. The proposed SDI quantifies progressive damper degradation from a single chassis-mounted accelerometer using fixed-coefficient signal processing and statistical analysis. A 15 s persistence criterion effectively rejects transient road disturbances, while the thermal model provides an independent indication of accumulated damper wear. The combination of the vibration and temperature-based channels through decision fusion achieves a 100% overall fault detection rate across the evaluated operating conditions.

The proposed framework was further evaluated under different road classes, vehicle speeds, payloads, sensor-noise levels, and progressive wear conditions. The results show that the thermal channel provides consistent fault detection, whereas the SDI offers complementary information on vibration behaviour. Parameter sensitivity analysis established appropriate values for the MAD multiplier, persistence duration, and fusion weights, while the benchmark comparison highlighted the benefit of combining vibration and temperature-based information rather than relying on either indicator alone.

The proposed algorithm has linear computational complexity and a small memory requirement, making it suitable for real-time embedded implementation using a single chassis-mounted accelerometer. Future work will focus on experimental validation using a suspension test rig or an in-vehicle platform, embedded implementation with execution-time evaluation, extension to full-vehicle models, and assessment under real-world road conditions involving nonlinear damper degradation mechanisms.

Abbreviations

HI: Health Index

ISO: International Organization for Standardization

MAD: Median absolute deviation

RMS: Root mean square

SDI: Suspension Degradation Index

Declarations

Acknowledgments

The author acknowledges that the open access publication charges for this article were funded by VIT University, Vellore Campus, India.

Funding

No funding

Author contributions

Geetha Mani: Conceptualization, methodology, modelling, simulation, analysis, validation, writing, review and editing.

Competing interests

The author declares that there are no competing interests

Data availability

The simulation data generated and analysed during the current study are available from the corresponding author upon reasonable request.

Code availability

The simulation code used in this study is available from the corresponding author upon reasonable request.

Clinical Trial Registration

Not applicable. This study is based entirely on computer simulations and does not involve a clinical trial.

Ethics, Consent to Participate, and Consent to Publish: Not applicable**.**

References

[1] Jeong K, Choi S. Model-based sensor fault diagnosis of vehicle suspensions with a support vector machine. Int J Automot Technol. 2019;20(5):961–70. https://doi.org/10.1007/s12239-019-0090-z

[2] Badie K, El Youssfi N, Chalh Z, Dami L. Fault detection using a reduced order filter for active suspension systems represented by Takagi-Sugeno fuzzy models. In: Proceedings of the 7th Global Power, Energy and Communication Conference (GPECOM). IEEE; 2025. pp. 979–84. https://doi.org/10.1109/GPECOM65896.2025.11061999.

[3] El Youssfi N, Badie K, Dami L. Fault detection using an observer for active suspension systems represented by Takagi-Sugeno fuzzy models. Int J Adapt Control Signal Process. 2026;40(7):1514–23. https://doi.org/10.1002/acs.70082.

[4] Lozoya-Santos J, Tudón-Martínez JC, Morales-Menendez R, Ramírez-Mendoza R, Molina Gutierrez A. Fault detection for an automotive MR damper. IFAC Proc Vol. 2012;45(6):1023–8. https://doi.org/10.3182/20120523-3-RO-2023.00247.

[5] Słomczynski M, Radkowski S, Makowski M. Model of a quarter car suspension with a damper containing magnetorheological fluid and with damaged parts controlled by backstepping method. Energies. 2023;16(7):3044. https://doi.org/10.3390/en16073044

[6] Azadi S, Soltani A. Fault detection for passive suspension systems using wavelet transform. SAE Technical Paper 2007-01-2368. 2007. https://doi.org/10.4271/2007-01-2368

[7] Zhao Z, Wu B, Zhou T. Feature analysis of degradation signal of rolling stock lateral damper. Information. 2020;11(6):298. https://doi.org/10.3390/info11060298

[8] Yang F, Hua C, Mu J, Huang Y, Liu W, Dong D. Fault diagnosis of high-speed train suspension systems under variable speeds based on dynamic transfer loss weight-deep subdomain adaptation network. Adv Eng Inform. 2025; 64:103091. https://doi.org/10.1016/j.aei.2024.103091

[9] Sai SA, Venkatesh SN, Dhanasekaran S, Balaji PA, Sugumaran V, Lakshmaiya N, et al. Transfer learning-based fault detection for suspension system using vibrational analysis and radar plots. Machines. 2023;11(8):778. https://doi.org/10.3390/machines11080778

[10] Balaji PA, Sugumaran V. Fault detection of automobile suspension system using decision tree algorithms: a machine learning approach. Proc Inst Mech Eng E J Process Mech Eng. 2024;238(3):1206–17. https://doi.org/10.1177/09544089231152698.

[11] Shah R, Venkatesh SN, Balaji PA, Sugumaran V. Weightless neural network-based fault diagnosis in suspension system. FME Trans. 2024;52(1):115–27. https://doi.org/10.5937/fme2401115S

[12] Wright MA, Wright GL, Wright KG. Shock absorber health and condition monitoring device. US Patent 8,275,515. 2012. https://patents.google.com/patent/US8275515B2.

[13] Howard CQ, Sergiienko N, Gallasch G. Monitoring the age of vehicle shock absorbers. In: Proceedings of the International Conference on Science and Innovation for Land Power (ICSILP 2018); 5–6 September 2018; Adelaide, Australia. pp. 1–4.

[14] Xie F, Cao J, Ding E, Wan K, Yu X, Ke J, et al. Temperature rise characteristics of the valve-controlled adjustable damping shock absorber. Mech Ind. 2020; 21:111. https://doi.org/10.1051/meca/2019084.

[15] Hryciow Z, Rybak P, Gieleta R. The influence of temperature on the damping characteristic of hydraulic shock absorbers. Eksploat Niezawodn. 2021;23(2):346–51. https://doi.org/10.17531/ein.2021.2.14.

[16] Hryciow Z. An investigation of the influence of temperature and technical condition on the hydraulic shock absorber characteristics. Appl Sci. 2022;12(24):12765. https://doi.org/10.3390/app122412765.

[17] Avendano JC, Leander J, Karoumi R. Image-based concrete crack detection method using the median absolute deviation. Sensors. 2024;24(9):2736. https://doi.org/10.3390/s24092736.

[18] Short M, Twiddle J. An industrial digitalization platform for condition monitoring and predictive maintenance of pumping equipment. Sensors. 2019;19(17):3781. https://doi.org/10.3390/s19173781.

[19] International Organization for Standardization. ISO 8608:2016 Mechanical vibration – Road surface profiles – Reporting of measured data. Geneva: ISO; 2016.

[20] Múčka P. Simulated road profiles according to ISO 8608 in vibration analysis. J Test Eval. 2018;46(1):405–18. https://doi.org/10.1520/JTE20160265.

[21] Loprencipe G, Zoccali P. Use of generated artificial road profiles in road roughness evaluation. J Mod Transp. 2017;25(1):24–33. https://doi.org/10.1007/s40534-017-0122-1.